Optical Materials: X 11 (2021) 100074

Contents lists available at ScienceDirect

Optical Materials: X

journal homepage: www.journals.elsevier.com/optical-materials-x

Invited Article

(INVITED) Energy transfer processes in $Sr_3Tb(PO_4)_3$ eulytite-type materials singly doped with Nd^{3+} and Sm^{3+}

Veronica Paterlini [a], Xiaowu Hu [b], Fabio Piccinelli [b], Marco Bettinelli [b,*]

[a] Department of Materials and Environmental Chemistry, Stockholm University, 106 91, Stockholm, Sweden
[b] Luminescent Materials Laboratory, Department of Biotechnology, University of Verona and INSTM, UdR Verona, Strada Le Grazie 15, 37134, Verona, Italy

ARTICLE INFO

Keywords:
Energy transfer
Lanthanide ions
Luminescence
Phosphate materials
Spectroscopy

ABSTRACT

In this study the optical spectroscopy, the excited state dynamics and in particular the energy transfer $Tb^{3+}\rightarrow Ln^{3+}$ (Ln = Nd or Sm), have been investigated in detail in eulytite double phosphate hosts of the type $Sr_3Tb(PO_4)_3$ doped with 1 mol% Ln^{3+}. It has been found that for Ln=Nd and Sm, the energy transfer efficiency (η_T) is 0.76 and 0.73, respectively, thanks to the assistance of fast migration in the Tb^{3+} $^5D_4$ level. The pathway responsible for the transfer of excitation has been unambiguously identified in the case of $Sr_3Tb_{0.99}Nd_{0.01}(PO_4)_3$, whilst the situation is more complex for $Sr_3Tb_{0.99}Sm_{0.01}(PO_4)_3$, due to high density of the final Sm^{3+} states that could be involved. The $Tb^{3+}\rightarrow Nd^{3+}$ energy transfer has been tentatively attributed to the exchange interaction on the basis of the short transfer distance and multipolar selection rules.

1. Introduction

Energy transfer involving trivalent lanthanide ions in inorganic solids has been and still is a fundamental field in modern luminescence research [1]. The contribution provided to this area (and many others) by Professor George Blasse has been invaluable for the advancement of the understanding of energy transfer and migration processes involving luminescent ions (see for instance Refs. [2–7]). In particular, Prof. Blasse studied in detail the migration of excitation in concentrated materials, especially based on Gd^{3+}, Eu^{3+} and Tb^{3+} [7–10].

These investigations, among others, motivated us to perform in the last years a thorough study the mechanisms responsible for the $Tb^{3+}\rightarrow Eu^{3+}$ energy transfer [11–14] in concentrated eulytite compounds of the type $A_3Tb(PO_4)_3$ (A=Sr, Ba), belonging to a class of luminescent materials that was studied for the first time by Prof. Blasse [15]. In these materials, fast energy migration occurs among the $^5D_4$ level of Tb^{3+} ions. For these reasons, we found it interesting to extend the previous studies to energy transfer processes involving Tb^{3+} and other lanthanide ions, such as Nd^{3+} and Sm^{3+}, present as dopants in the eulytite $A_3Tb(PO_4)_3$, with the aim of understanding the impact of the various electronic structures of the co-dopants on the transfer mechanisms and rates. The results of this new investigation are presented and discussed here.

2. Experimental and structural data

The eulytite-type compounds $Sr_3Tb(PO_4)_3$ and $Sr_3Tb_{0.99}Ln_{0.01}(PO_4)_3$ (Ln=Nd, Sm) were obtained by solid state reaction at high temperature (1250 °C, 48 h) as described in Ref. [11].

X-ray diffraction patterns were measured using a Thermo ARL X'TRA powder diffractometer, in Bragg-Brentano geometry, with a Cu-anode as X-ray source and a Peltier Si(Li) cooled solid state detector. The XRD patterns were collected with a scan rate of 1.2°/min and an integration time of 1.5 s in the 5–90° 2θ range.

Luminescence spectra and decay curves were collected at room temperature with a Fluorolog 3 (Horiba-Jobin Yvon) spectrofluorometer. The equipment was composed by a Xe lamp, a double excitation monochromator and a single emission monochromator (mod. HR320). The emitted signal was detected by means of a photomultiplier in the photon counting mode. For the measurement of the decay curves, time correlated single photon counting technique (TCSPC) was used, with a xenon microsecond pulsed lamp as excitation source. The decays curves were fitted by an appropriate software. For the IR measurements, a linear InGaAs detector working up to 1700 nm was used (512 pixels, 50x500μm).

* Corresponding author.
E-mail address: marco.bettinelli@univr.it (M. Bettinelli).

https://doi.org/10.1016/j.omx.2021.100074
Received 1 June 2021; Accepted 3 June 2021
Available online 17 June 2021

3. Results and discussion

3.1. Structural investigation

Single eulytite-type phases were obtained for all the synthesized eulytite double phosphates [$Sr_3Tb(PO_4)_3$ and $Sr_3Tb_{0.99}Ln_{0.01}(PO_4)_3$, Ln=Nd and Sm], as confirmed by powder X-ray diffraction (XRD). In Fig. 1, the patterns of the samples are presented; all the diffraction peaks belong to eulytite structure and no impurity phases are observed.

It is well known that eulytite double phosphates with the formula $A_3M(PO_4)_3$ (A=Ca, Sr, Ba; M=La-Lu, Y, Bi) are cubic (space group $I\bar{4}3d$) and isomorphous with the mineral eulytine ($Bi_4Si_3O_{12}$) [15,16]. The crystal structures of the materials under investigation have been recently described [13]. The partial substitution of Tb^{3+} with 1 mol% of another lanthanide ion (in the present study Nd^{3+} or Sm^{3+}) has a negligible impact on the cell parameter of the doped phase with respect to the undoped one.

3.2. Luminescence spectroscopy

3.2.1. $Sr_3Tb(PO_4)_3$ eulytite doped with Nd^{3+}

The luminescence spectra of the $Sr_3Tb_{0.99}Nd_{0.01}(PO_4)_3$ eulytite are shown in Fig. 2(a) and (b) in the visible and NIR regions, respectively.

The excitation spectrum of the emission observed at 542 nm is shown in the Fig. 2(a). Irradiation in the near UV is bound to excite in practice only Tb^{3+}, since its concentration is 99 times higher than the one of Nd^{3+}. The visible emission spectrum obtained upon excitation in the levels above $^5D_3$ (close to 350 nm) is dominated by emission from the $^5D_4$ level of Tb^{3+} (Figure 2a); no emission from $^5D_3$ is observed due to efficient cross relaxation leading to fully non-radiative $^5D_3 \rightarrow {}^5D_4$ decay. Conversely, excitation at the same wavelength gives rise to emission bands in the NIR region that are clearly assigned to transitions originating from the $^4F_{3/2}$ level of Nd^{3+} to lower lying ^4I_J (J=9/2, 11/2, 13/2) (Fig. 2(b)). This indicates that $Tb^{3+} \rightarrow Nd^{3+}$ energy transfer is present. The $^4F_{3/2}$ emitting level is populated by multiphonon relaxation from $^4G_{5/2}$ (see below) across the levels located in between, since the eulytite phosphate host has high energy phonons available (up to 900 cm^{-1}) [17,18].

This observation agrees with the conclusions drawn by Nakazawa and Shionoya in their study about energy transfer between rare earth ions in $Ca(PO_3)_2$ glass [19], who attributed this process to the resonant mechanism:

$$^5D_4(Tb^{3+}) + {}^4I_{9/2}(Nd^{3+}) \rightarrow {}^7F_4(Tb^{3+}) + {}^4G_{5/2}(Nd^{3+}). \quad (1)$$

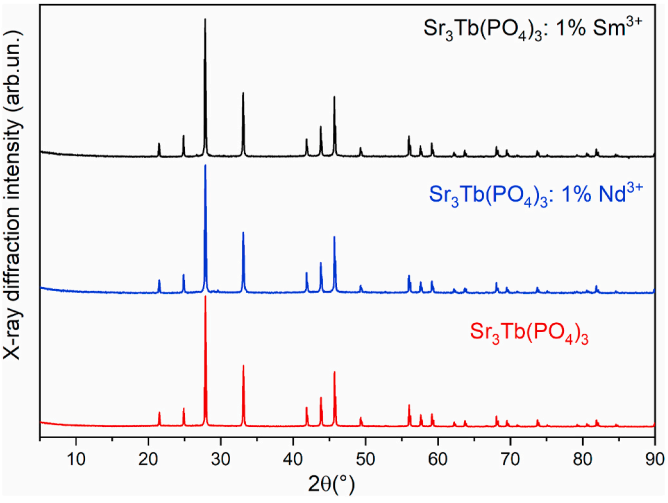

Fig. 1. X-ray diffraction powder patterns of undoped and doped $Sr_3Tb(PO_4)_3$ samples.

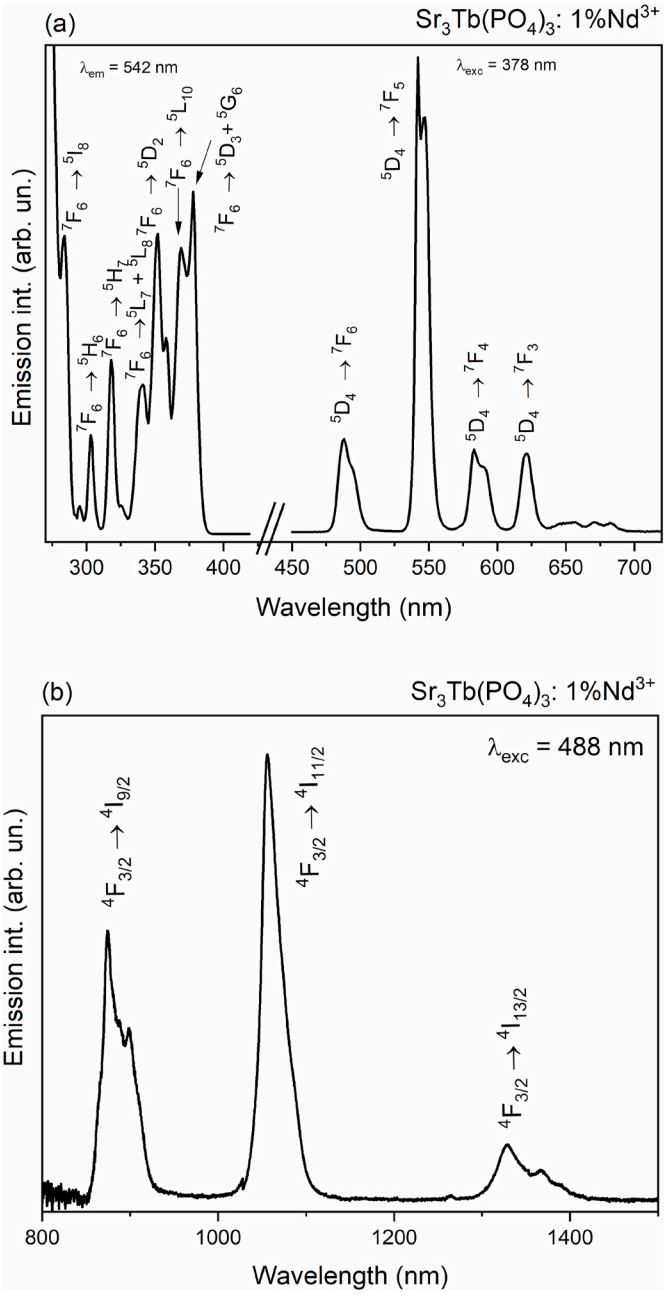

Fig. 2. (a) Visible RT emission spectrum of $Sr_3Tb_{0.99}Nd_{0.01}(PO_4)_3$ with excitation at 378 nm. (b) NIR RT emission spectrum of $Sr_3Tb_{0.99}Nd_{0.01}(PO_4)_3$ with excitation at 488 nm.

In Fig. 3, the mechanism responsible for the population of Nd^{3+} $^4F_{3/2}$ emitting level by energy transfer from $^5D_4$ level of Tb^{3+} is depicted.

The decay curve of the $^5D_4$ level of Tb^{3+}, measured upon pulsed excitation at 378 nm, is shown in Fig. 4.

The profile is exponential with a decay constant $\tau_{Tb\text{-}Nd}$=0.64 ms, compared with the value τ_{Tb}=2.68 ms obtained for neat $Sr_3Tb(PO_4)_3$ [11]. This indicates that the $Tb^{3+} \rightarrow Nd^{3+}$ occurs following fast energy migration in the Tb^{3+} subset of ions ($^5D_4$ level) [13,20].

The effective energy transfer probability k_{ET} can be estimated from the expression [21]:

$$1/\tau_{Tb\text{-}Nd} = 1/\tau_{Tb} + k_{ET} \quad (2)$$

where τ_{Tb} and $\tau_{Tb\text{-}Nd}$ are the $^5D_4$ decay times in the absence and in the presence of the Nd^{3+} dopant. The resulting value is k_{ET}(Tb→Nd)=

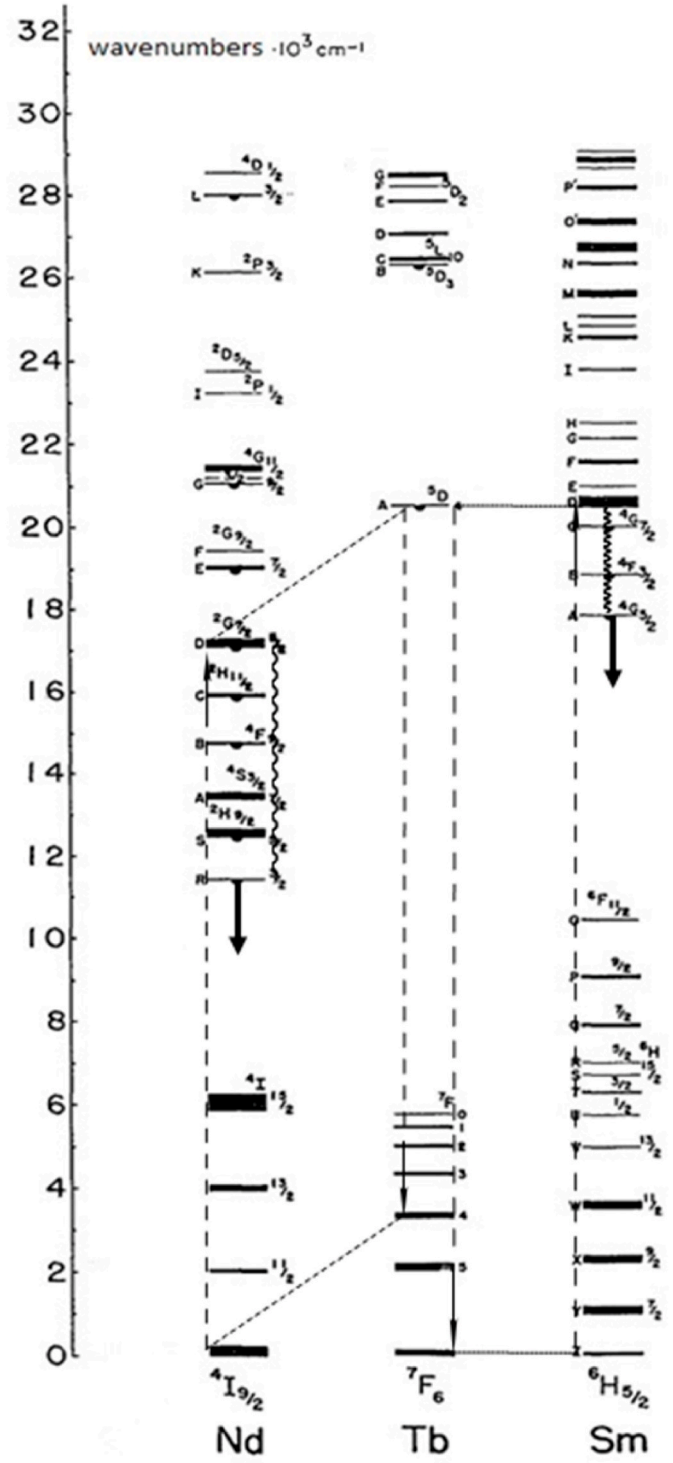

Fig. 3. Dieke diagram of the energy levels arising from $4f^n$ configurations of Nd^{3+}, Tb^{3+} and Sm^{3+}. The population mechanism of the Nd^{3+} $^4F_{3/2}$ and Sm^{3+} $^4G_{5/2}$ emitting levels by energy transfer from the $^5D_4$ level of Tb^{3+} is also reported. Adapted from G. H. Dieke, H. M. Crosswhite, The Spectra of the Doubly and Triply Ionized Rare Earths, Appl. Opt. 2 (1963) 675–686.

1.19×10^3 s^{-1}. Additionally, the energy transfer efficiency η_T can be estimated using [22]:

$$\eta_T = 1 - \tau_{Tb\text{-}Nd}/\tau_{Tb} \quad (3)$$

and the value $\eta_T(Nd)=0.76$ is found. The transfer efficiency is relatively high; slightly larger values were found for $Sr_3Tb(PO_4)_3$ and Ba_3Tb

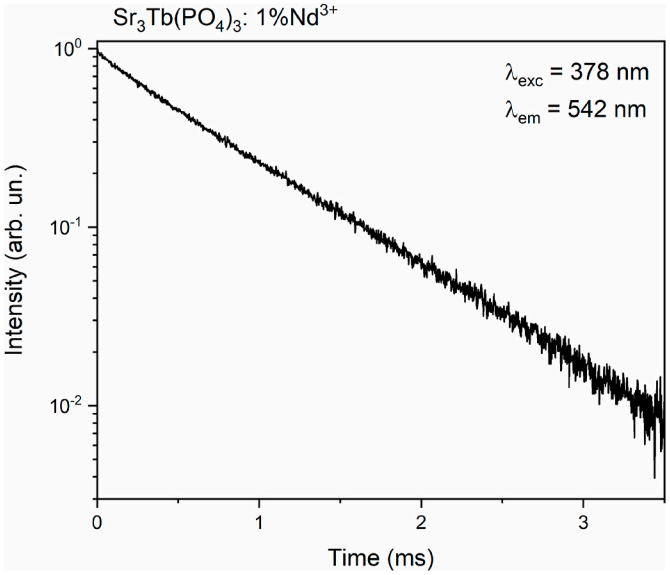

Fig. 4. Room temperature $^5D_4$ decay curve of Tb^{3+} (λ_{exc} = 378 nm) in $Sr_3Tb_{0.99}Nd_{0.01}(PO_4)_3$.

$(PO_4)_3$:Eu^{3+} in which the doping level was ten times higher [14]. The material is able to convert UV-visible excitation to NIR emission from $^4F_{3/2}$, but it must noted that significant non-radiative losses are predicted to occur through the almost resonant back-transfer process:

$$^7F_6(Tb^{3+}) + {}^4F_{3/2}(Nd^{3+}) \rightarrow {}^7F_1(Tb^{3+}) + {}^4I_{15/2}(Nd^{3+}). \quad (4)$$

The study of this transfer lies beyond the scope of this paper, as our present experimental facilities do not allow us to measure the decay of $^4I_{15/2}(Nd^{3+})$ upon pulsed excitation.

3.2.2. *$Sr_3Tb(PO_4)_3$ eulytite doped with Sm^{3+}*

As shown in Fig 5a, the room temperature visible emission spectrum of $Sr_3Tb_{0.99}Sm_{0.01}(PO_4)_3$ measured upon excitation at 402 nm ($^4F_{7/2}$ level of Sm^{3+}) shows four well defined emission bands assigned to transitions from the $^4G_{5/2}$ level of Sm^{3+}, which is populated by multi-phonon relaxation, and terminating onto the final levels ^6H_J, with J=5/2 (peaking at 564 nm), 7/2 (598 nm), 9/2 (645 nm) and 11/2 (705 nm) [23].

On the other hand, the emission spectrum excited at 378 nm shows two additional main bands, peaking at 488 and 542 nm and assigned to the $^5D_4 \rightarrow {}^7F_6$ and $^5D_4 \rightarrow {}^7F_5$ transitions of Tb^{3+}, respectively. The emission spectrum obtained upon excitation at 485 nm shows the same bands as for λ_{exc}=378 nm, apart from the $^5D_4 \rightarrow {}^7F_6$ which is resonant with the excitation. Sm^{3+} does not appear to be excited at this latter wavelength, although absorption in this region has been reported [24]. As noted above in the case of Nd^{3+}-doped sample, Tb^{3+} concentration is 99 times higher than the one of Sm^{3+}, and therefore its excitation can be considered as negligible. Fig. 5b shows the NIR emission spectrum measured at RT upon excitation at 488 nm. The bands peaking at 903, 946, 1028, 1176 and 1413 nm are assigned to transitions from the $^4G_{5/2}$ level of Sm^{3+} to the levels ^6H_J (J=5/2–11/2) respectively [25].

Fig. 6 shows the excitation spectrum of the sample under investigation measured with λ_{em} =542, 598 and 645 nm.

The emission at 542 nm does not correspond to any excitation transition related to Sm^{3+}, and the relevant excitation spectrum presents the typical features of Tb^{3+} in eulytites [11], with dominant peaks at 378 and 488 nm, corresponding to transitions to the $^5D_3$ and $^5D_4$ levels. On the other hand, the excitation spectra measured with λ_{em}=598 and 645 nm shows both Sm^{3+}-related features, such as the peak at 402 nm ($^6H_{5/2} \rightarrow {}^4F_{7/2}$) and the structure located in the region 420–475 nm, and Tb^{3+}-related peaks, such as the ones in the UV region, and especially at

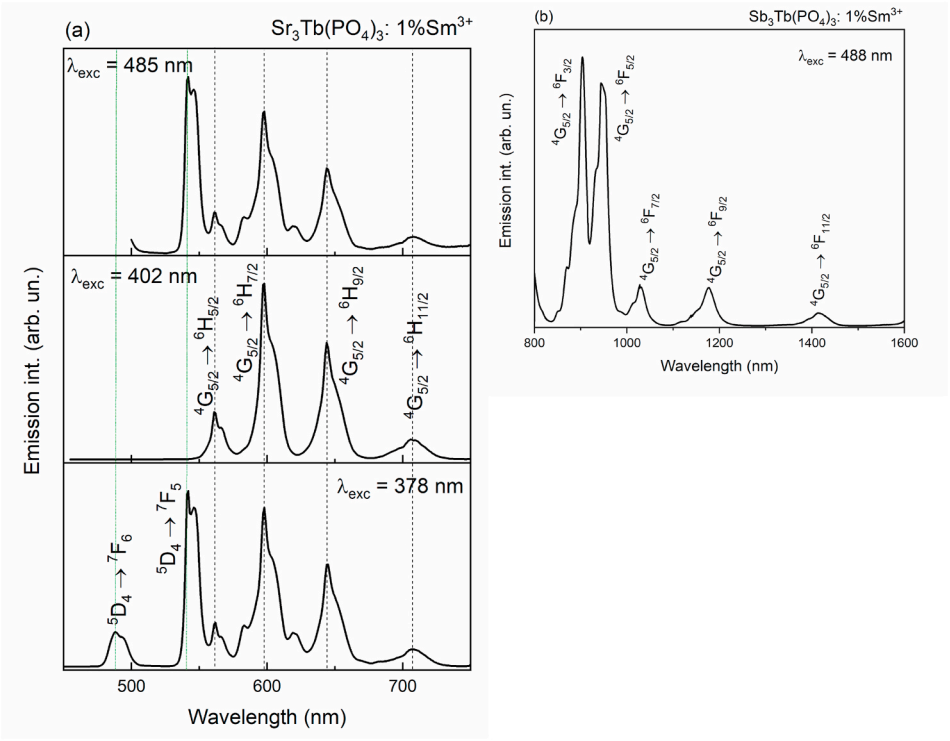

Fig. 5. (a) Visible RT emission spectrum of $Sr_3Tb_{0.99}Sm_{0.01}(PO_4)_3$ with excitation at 378 , 402 and 485 nm. (b) NIR RT emission spectrum of $Sr_3Tb_{0.99}Sm_{0.01}(PO_4)_3$ with excitation at 488 nm.

378 and 488 nm. It is therefore clear that $Tb^{3+} \rightarrow Sm^{3+}$ energy transfer takes place, as documented for other oxide materials (see for example [24,26]).

The process responsible for the energy transfer process is assigned as

$$^5D_4(Tb^{3+}) + {}^6H_{5/2}(Sm^{3+}) \rightarrow {}^7F_6(Tb^{3+}) + {}^4I_{9/2}, {}^4G_{7/2}\ (Sm^{3+}), \quad (5)$$

on the basis of the energy level diagrams of the two ions [27], and the spectral overlap between the excitation of Sm^{3+} and the emission of Tb^{3+} in the region between 480 and 500 nm [24]. The $^4I_{9/2}$,$^4G_{7/2}$ rapidly relax to the emitting $^4G_{5/2}$ level through multiphonon relaxation (see Fig. 3).

The room temperature decay curves of the luminescence in the visible region, after pulsed excitation of $Sr_3Tb_{0.99}Sm_{0.01}(PO_4)_3$, are shown in Fig. 7.

The decay profile of the $^5D_4$ level of Tb^{3+} is almost perfectly exponential with a decay constant of 0.73 ms. The decay is significantly faster than for neat $Sr_3Tb(PO_4)_3$ (2.68 ms) due to energy transfer to Sm^{3+}. As expected, the exponential profile clearly indicates that the transfer process occurs in the presence of fast migration among the $^5D_4$ levels of Tb^{3+}. Using equations (2) and (3) the values k_{ET}(Tb→Sm)=9.97×10^2 s^{-1} and η_T(Sm)=0.73 are obtained, quite similar to the ones obtained for the transfer involving the Nd^{3+} dopant.

As for the RT decay curves of the $^4G_{5/2}$ level of Sm^{3+}, the one obtained upon direct excitation at 402 nm, corresponding to the $^4F_{7/2}$ level, and observation at 598 nm (transition $^4G_{5/2} \rightarrow {}^6H_{7/2}$) is almost exponential with a decay constant for $^4G_{5/2}$ of 2.19 ms, with a minor faster component at short times of about 0.7–0.8 ms, attributed to a small degree of overlapping with the $^5D_4 \rightarrow {}^7F_4$ transition of Tb^{3+}. For the sake of comparison, the decay of $^4G_{5/2}$ in diluted $Sr_3Y(PO_4)_3$:1 mol% Sm^{3+} was measured by us to be exponential with a decay time of 2.74 ms (not shown), whilst in the similar host $Ba_3Lu(PO_4)_3$:1 mol% Sm^{3+} it was estimated to be 2.32 ms [20]. The temporal profiles of the $^4G_{5/2}$ emission upon excitation at 378 ($^5D_3$) and 488 nm ($^5D_4$) are perfectly superimposable, and show a well evident rise, followed by an exponential decay with a time constant of 2.17 ms. The exponential build-up of the emission at short times after the pulsed excitation has a time constant of about 0.50 ms and is attributed to the feeding of by $^5D_4$ due to the energy transfer process; this confirms the conclusions drawn above about the transfer process. It is worth noting that the emission from the $^4G_{5/2}$ level of Sm^{3+} cannot be quenched from any efficient back energy transfer to Tb^{3+}, due to energy mismatch of the states involved.

A comparison between the resulting colours in the two materials is shown in the CIE diagrams (Fig. 8).

Since Nd^{3+} presents emission only in the NIR region upon excitation into the $^5D_3$ level of Tb^{3+}, only the green feature of Tb^{3+} is obtained for Nd^{3+}-doped material. Conversely, upon the same excitation, both Tb^{3+} and Sm^{3+} emission are present in the visible region, with a domination of the latter. Therefore, the obtained colour is located in the orange region. Similar CIE are obtained when the same sample is excited at 485 nm as in this case, clearly the emission band at 485 nm, that is resonant with the excitation, does not contribute to the final emission spectrum, leading to a slight shift in the CIE coordinates but always in the orange region). Finally, at 402 nm, Sm^{3+} ion is selectively excited and the final spectrum in the visible region results in a red colour due to sole emission of this ion.

3.2.3. *Impact of the crystal structure on the energy transfer mechanism*

Details about the crystal structure of the materials under investigation have been reported before [13,14,16]. There is only one site for both divalent and trivalent cations with coordination number 9 and point symmetry C_3. The A^{2+}/M^{3+} cations are located in a disordered way in a single crystallographic site, with a relative occupation of 0.75/0.25. As reported in section 3.1, the lattice parameters are in practice constant after dilute substitution of Tb^{3+} with Nd^{3+} or Sm^{3+} (doping) due to the close similarity of their ionic radii (1.095 Å for Tb^{3+}, 1.163 Å for Nd^{3+} and 1.132 Å for Sm^{3+} in 9-fold coordination) [28].

As for the local environment of the cations, Each A^{2+}/M^{3+} ion is surrounded by other identical 11 nearest neighbour A^{2+}/M^{3+} cationic sites. Therefore, due to the abovementioned occupation factors, one trivalent ion on average is surrounded by 11 × 0.25=2.75 trivalent near

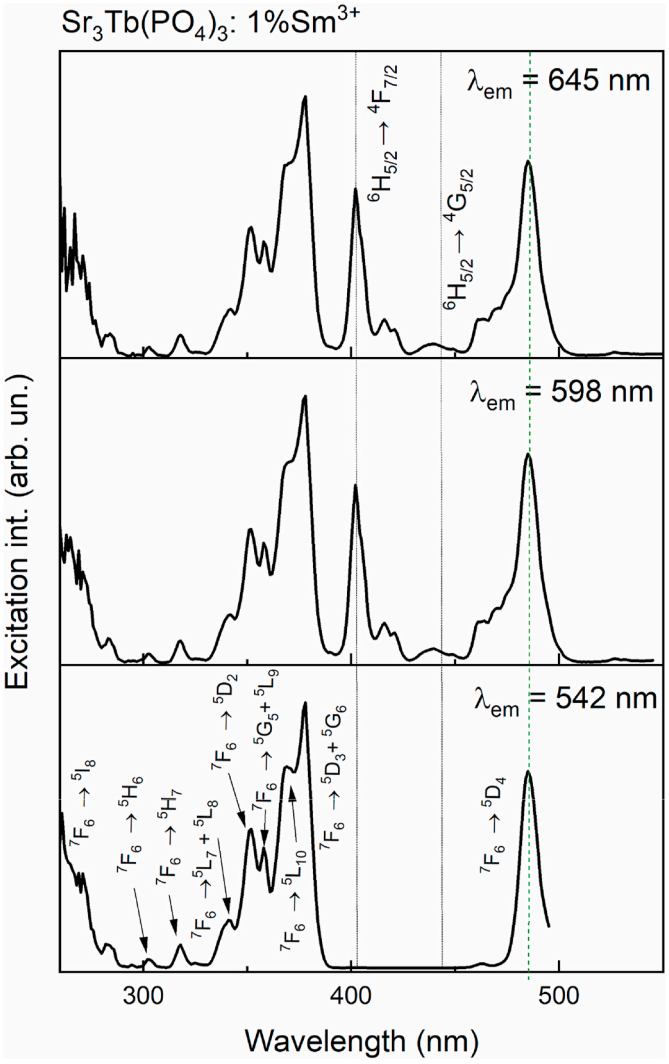

Fig. 6. RT excitation spectrum of $Sr_3Tb_{0.99}Sm_{0.01}(PO_4)_3$ measured with λ_{em} =542, 598 and 645 nm.

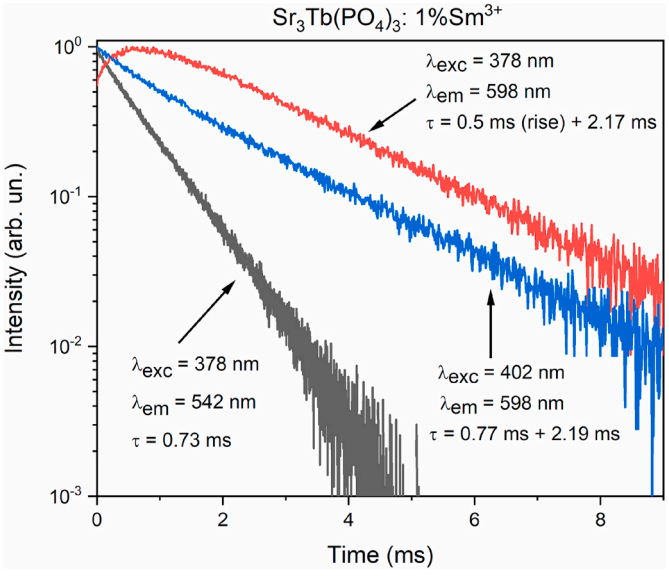

Fig. 7. RT decay curves of the luminescence in the visible region, after pulsed excitation of $Sr_3Tb_{0.99}Sm_{0.01}(PO_4)_3$.

neighbour ions. This implies that in the neat terbium eulytite each Tb^{3+} ion has 2.75 Tb^{3+} nearest neighbours, and in the Tb/Ln materials 2.722 Tb^{3+} and 0.028 Ln^{3+} ions nearest neighbour ions (Ln=Nd, Sm). In the presence of the Ln^{3+} dopant the crystallographic positions of the atoms are unchanged and so the distances Tb^{3+}–Tb^{3+} and Tb^{3+}–Ln^{3+} are considered identical. In a previous paper [14] we have reported that in the same host the distances between a reference cation and the nearest neighbour ones have three possible values, i.e. 3.971(2) Å (x3), 4.378(1) Å (x2) and 4.754(1) Å (x6). We can safely adopt these values for the nearest neighbour Tb^{3+}–Nd^{3+} and Tb^{3+}–Sm^{3+} distances in the materials under investigation. As migration among the $^5D_4$ levels of Tb^{3+} is very fast, the excitation will reach a donor ion which has at least one Nd^{3+} or Sm^{3+} ion in a nearest neighbour position. This implies that the energy transfer process presumably occurs across a short distance (3.971–4.754 Å), and that short-range interactions, such as electric quadrupole-electric quadrupole (EQ-EQ) and/or exchange, could play a dominant role.

In fact, in the case of the Tb^{3+}→Eu^{3+} energy transfer in Sr, Sr/Ba and Ba-eulytites, Carneiro Neto et al. have recently shown, through the comparison of detailed theoretical calculations and experimental data derived from luminescence spectroscopy, that these hypotheses are indeed correct [14]. Presumably, a similar situation occurs for the materials under investigation. At this stage, a few comments can be made. In the case of the Tb^{3+}→Sm^{3+} transfer, the final states for Sm^{3+} lie in an energy region that very dense with levels, and at least two states [$^4I_{9/2}$,$^4G_{7/2}$ (Sm^{3+})] are involved; this makes a simple analysis unfeasible in the absence of detailed theoretical calculations. On the other hand, the Tb^{3+}→Nd^{3+} is much simpler and more amenable to some considerations.

The transfer mechanism (1) in the past has been assigned, in a Ca $(PO_3)_2$ glass doped with low amounts of Tb^{3+} (3%) and Nd^{3+} (0.1–3%), to the electric dipole-electric quadrupole interaction [19,29]. In the present case, given the short transfer distance and the previous theoretical results on the Tb^{3+}→Eu^{3+} case, this mechanism presumably is not the dominant one. On the other hand, the low values of the squared reduced matrix elements of the unit tensor operator $<||U^{(\lambda)}||>^2$ (for λ=2, 4, 6) for the $^5D_4$→$^7F_4$ of Tb^{3+} [27] do not appear to be compatible with an EQ-EQ interaction, since this requires high values of $<||U^{(2)}||>^2$ for the transitions involved in the two optical centres [30]. For this reason, we tentatively attribute the transfer to exchange interaction, being aware that detailed theoretical calculations are required in order to obtain a full understanding of the transfer mechanism.

4. Conclusions

Energy transfer processes of the types Tb^{3+}→Nd^{3+} and Tb^{3+}→Sm^{3+} have been studied at room temperature in eulytite double phosphate materials with stoichiometry $Sr_3Tb_{0.99}Nd_{0.01}(PO_4)_3$ and $Sr_3Tb_{0.99}Sm_{0.01}(PO_4)_3$. As already found for $(Ba,Sr)_3Tb_{1-x}Eu_x(PO_4)_3$, the transfer of excitation from the Tb^{3+} to the dopant is assisted by very fast energy migration in the $^5D_4$ subset of levels, and effectively occurs between nearest neighbour ions. For this reason, the transfer efficiency results to be high compared to what observed in other hosts. The transfer mechanisms have been identified for both dopant ions and, in the simpler case of the Nd^{3+} acceptor, there are indications that the short-range transfer process, occurring for distances close to 4 Å, is mainly due to the exchange interaction requiring wavefunction overlap. This agrees with the rule of thumb proposed by Blasse and Grabmaier for Ln^{3+} ions, allowing exchange for donor-acceptor distances lower than 5 Å [20]. The present indication should clearly be corroborated by detailed theoretical calculations. As a last remark, we note that, in the materials under investigation. downshifting from the near UV and the visible regions to the near IR [31] can be obtained. The efficiency of this process remains to be ascertained in the case of the eulytite activated with Nd^{3+}.

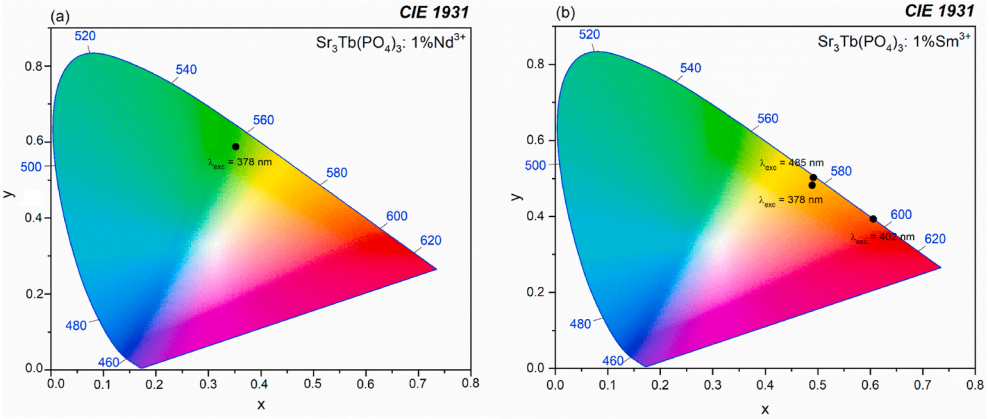

Fig. 8. CIE diagrams for (a) $Sr_3Tb_{0.99}Nd_{0.01}(PO_4)_3$ and (b) $Sr_3Tb_{0.99}Sm_{0.01}(PO_4)_3$ samples.

Funding

This work was supported by the Department of Biotechnology, Univ. Verona, Italy, through the FUR funding scheme.

Declaration of competing interest

The authors declare that they have no known competing financial interests or personal relationships that could have appeared to influence the work reported in this paper.

Acknowledgements

The authors gratefully thank Erica Viviani (Univ. Verona) for expert technical assistance and the Facility "Centro Piattaforme Tecnologiche" of the University of Verona for access to the Fluorolog 3 (Horiba-Jobin Yvon) spectrofluorometer and Thermo ARL X'TRA powder diffractometer. X. W. thanks China Scholarship Council (CSC) (fund No.201906130187) for the 3-years study in Italy as a PhD. student.

References

[1] B. Di Bartolo, Energy Transfer Processes in Condensed Matter, Plenum, New York and London, 1983.
[2] G. Blasse, Energy transfer in oxidic phosphors, Phys. Lett. A 28 (1968) 44–445.
[3] G. Blasse, Energy transfer between inequivalent Eu^{2+} ions, J. Solid State Chem. 62 (2) (1986) 207–211.
[4] G. Blasse, Luminescence of inorganic solids: from isolated centres to concentrated systems, Prog. Solid State Chem. 18 (1988) 79–171.
[5] M. Buijs, A. Meyerink, G. Blasse, Energy transfer between Eu^{3+} ions in a lattice with two different crystallographic sites: Y_2O_3:Eu^{3+}, Gd_2O_3:Eu^{3+} and Eu_2O_3, J. Lumin. 37 (1987) 9–20.
[6] G. Blasse, Energy transfer from Ce^{3+} to Eu^{3+} in (Y, Gd)F_3, Phys. Status Solidi A 75 (1983) K41–K43.
[7] A.J. De Vries, M.F. Hazenkamp, G. Blasse, On the Gd^{3+} luminescence and energy migration in Li(Y, Gd)F_4-Tb^{3+}, J. Lumin. 42 (1988) 275–282.
[8] F. Kellendonk, G. Blasse, Luminescence and energy transfer in $EuAl_3B_4O_{12}$, J. Chem. Phys. 75 (1981) 561–571.
[9] F. Kellendonk, G. Blasse, Luminescence and energy transfer in $TbAl_3B_4O_{12}$, J. Phys. Chem. Solid. 43 (1982) 481–490.
[10] G. Blasse, Energy migration in rare-earth compounds, Recl. Trav. Chim. Pays-Bas 105 (1986) 143–149.
[11] M. Bettinelli, A. Speghini, F. Piccinelli, J. Ueda, S. Tanabe, Energy transfer processes in $Sr_3Tb_{0.90}Eu_{0.10}(PO_4)_3$, Opt. Mater. 33 (2010) 119–122.
[12] M. Bettinelli, F. Piccinelli, A. Speghini, J. Ueda, S. Tanabe, Excited state dynamics and energy transfer rates in $Sr_3Tb_{0.90}Eu_{0.10}(PO_4)_3$, J. Lumin. 132 (2012) 27–29.
[13] V. Paterlini, F. Piccinelli, M. Bettinelli, Tb^{3+}→Eu^{3+} energy transfer processes in eulytite $A_3Tb(PO_4)_3$ (A=Sr, Ba) and silico-carnotite $Ca_3Tb_2Z_3O_{12}$ (Z=Si, Ge) materials doped with Eu^{3+}, Phys. B (Amsterdam, Neth.) (2019) 575, art. n. 411685.
[14] A.N. Carneiro Neto, R.T. Moura, A. Shyichuk, V. Paterlini, F. Piccinelli, M. Bettinelli, O.L. Malta, Theoretical and experimental investigation of the Tb^{3+}→Eu^{3+} energy transfer mechanisms in cubic $A_3Tb_{0.90}Eu_{0.10}(PO_4)_3$ (A = Sr, Ba) materials, J. Phys. Chem. C 124 (2020) 10105–10116.
[15] G. Blasse, New compounds with eulytine structure: crystal chemistry and luminescence, J. Solid State Chem. 2 (1970) 27–30.
[16] J. Barbier, Structural refinements of eulytite-type $Ca_3Bi(PO_4)_3$ and $Ba_3La(PO_4)_3$, J. Solid State Chem. 101 (1992) 249–256.
[17] I.L. Botto, A correlation between crystallographic and spectroscopic data for some eulytite-type phosphates containing bismuth, Spectrochim. Acta, Part A 43 (1987) 119–121.
[18] F. Piccinelli and M. Giarola, unpublished results.
[19] E. Nakazawa, S. Shionoya, Energy transfer between trivalent rare earth ions in inorganic solids, J. Chem. Phys. 47 (1967) 3211–3219.
[20] G. Blasse, B.C. Grabmaier, Luminescent Materials, Springer-Verlag, 1994. Chapter 5.
[21] R. Reisfeld, Y. Kalisky, Energy transfer between Bi^{3+} and Nd^{3+} in germanate glass, Chem. Phys. Lett. 50 (1977) 199–201.
[22] R. Reisfeld, N. Lieblich-Soffer, Energy transfer from UO_2^{2+} to Sm^{3+} in phosphate glass, J. Solid State Chem. 28 (1979) 391–395.
[23] Z. Yang, D. Xu, J. Sun, Synthesis and luminescence properties of $Ba_3Lu(PO_4)_3$:Sm^{3+} phosphor for white light emitting diodes, Opt Express 25 (2017) A391–A401.
[24] L. Yao, G. Chen, T. Yang, Y. Luo, Y. Yang, Optical properties and energy transfer in Tb^{3+}/Sm^{3+} co-doped Na_2O-CaO-P_2O_5-B_2O_3-ZrO_2 glasses, J. Alloys Compd. 692 (2017) 346–350.
[25] A. Herrera, R.G. Fernandes, A.S.S. de Camargo, A.C. Hernandes, S. Buchner, C. Jacinto, N.M. Balzaretti, Visible–NIR emission and structural properties of Sm^{3+} doped heavy-metal oxide glass with composition B_2O_3–PbO–Bi_2O_3–GeO_2, J. Lumin. 171 (2016) 106–111.
[26] X. Sun, Z. Huang, Y. Guo, S. Zhou, K. Liu, Tb^{3+}→Sm^{3+} energy transfer induced tunable luminescence in $Ba_3MgSi_2O_8$:Tb^{3+}/Sm^{3+} phosphors, J. Lumin. 219 (2020) 116925.
[27] W.T. Carnall, H. Crosswhite, H.M. Crosswhite, Energy Level Structure and Transition Probabilities in the Spectra of the Trivalent Lanthanides in LaF_3, Report ANL-78-XX-95, Argonne National Lab. (ANL), Argonne, IL (United States), 1978.
[28] R.D. Shannon, Revised effective ionic radii and systematic studies of interatomic distances in halides and chalcogenides, Acta Crystallogr. A32 (1976) 751–767.
[29] K. Tonooka, K. Yamada, N. Kamata, F. Maruyama, Role of the dipole-quadrupole interaction in fluorescence of RE glasses estimated by Monte Carlo simulation, J. Lumin. 60–61 (1994) 864–866.
[30] T.T. Basiev, Yu V. Orlovskii, Yu S. Privis, High-order multipole interaction in nanosecond Nd-Nd energy transfer, J. Lumin. 69 (1996) 187–202.
[31] W.G.J.H.M. van Sark, A. Meijerink, R.E.I. Schropp, Solar spectrum conversion for photovoltaics using nanoparticles, in: Vasilis Fthenakis (Ed.), Third Generation Photovoltaics, IntechOpen Limited, London, UK, 2012. Chapter 1.